Frazao, L., Velthuis, J., Thomay, C., & Steer, C. (2016). Discrimination of high-Z materials in concrete-filled containers using Muon Scattering Tomography. *Journal of Instrumentation*, *11*. https://doi.org/10.1088/1748-0221/11/07/P07020

Peer reviewed version

Prepared for submission to JINST

Discrimination of high-Z materials in concrete-filled containers using Muon Scattering Tomography

L. Frazão,[a,1] **J. Velthuis,**[a] **C. Thomay**[a] **and C. Steer**[b]

[a] *University of Bristol, H. H. Wills Physics Laboratory, Tyndall Avenue, Bristol, BS8 1TL, United Kingdom*
[b] *AWE, Aldermaston, Reading, RG7 4PR, United Kingdom*

E-mail: leonor.frazao@bristol.ac.uk

Abstract: An analysis method of identifying materials using muon scattering tomography is presented, which uses previous knowledge of the position of high-Z objects inside a container and distinguishes them from similar materials. In particular, simulations were performed in order to distinguish a block of Uranium from blocks of Lead and Tungsten of the same size, inside a concrete-filled drum. The results show that, knowing the shape and position from previous analysis, it is possible to distinguish $5 \times 5 \times 5$ cm^3 blocks of these materials with about 4h of muon exposure, down to $2 \times 2 \times 2$ cm^3 blocks with 70h of data using multivariate analysis (MVA). MVA uses several variables, but it does not benefit the discrimination over a simpler method using only the scatter angles. This indicates that the majority of discrimination is provided by the angular information. Momentum information is shown to provide no benefits in material discrimination.

Keywords: Search for radioactive and fissile materials; Pattern recognition, cluster finding, calibration and fitting methods; Particle tracking detectors (Gaseous detectors)

[1]Corresponding author.

Contents

1 Introduction

Muon scattering tomography (MST) was first developed as an alternative to X-ray imaging of cargo containers [1], using cosmic-ray muons instead. Their main advantages are the fact that they are a natural source, present all over Earth's surface, that they are highly penetrating, even in dense and big objects, not possible with X-rays, and that it is not possible to trigger against the scanning. MST is particularly useful to determine the content of containers without opening them or introducing additional radiation.

Cosmic muons have been used to scan objects such as cargo containers [2], nuclear waste containers [3] and geological formations [4]. This paper shows a study of the application of muon scattering tomography to improve material identification, using the particular example of a nuclear waste container. This is important in the case of legacy nuclear waste, because some containers contain unknown materials, or materials which have changed over time, for example with some materials expanding, or some new material being produced. In order to proceed with the waste disposal and assess the respective costs, it is necessary to know what materials each vessel contains.

Some attempts at material identification have been made before, for example in [5], but for high-Z materials, such as lead and denser objects this distinction has not been possible.

The present work is based on the assumption that it is possible to know the shape and position of high-Z materials in a background material with a lower Z. This is possible using several different methods, such as the one described in [6], [5], [7] and [8]. In [9] a method is described to identify

the edges of small blocks of material inside concrete, with a precision of 1.20 ± 0.37 mm. Hence, it is possible to find lumps and using this technique as a second step to find their edges. The next step in identifying the material would be comparing the object of interest to data from known typical high-Z materials, to find which most resembles the unknown material. It is shown in this paper that by selecting the tracks that passed through the high-Z material and comparing them for different materials, we are able to distinguish those materials. We compare typical waste fuel material, uranium, with benign shielding materials of tungsten and lead.

1.1 Muon Scattering Tomography

Muon scattering tomography is a technique which uses the muons present in natural cosmic radiation as probes to scan objects like nuclear waste drums or cargo containers.

Muons undergo multiple scattering in matter [10, 11], where the 2D projected scattering angle distribution is approximately Gaussian, with width σ dependent on the radiation length of the material traversed,

$$\sigma \approx \frac{13.6 \text{ MeV}}{\beta c p} z \sqrt{X/X_0}(1 + 0.038 \ln(X/X_0)), \tag{1.1}$$

where p is the momentum of the muon, βc its velocity, z its charge number, X the thickness of the material, and X_0 the radiation length [12] which is given by

$$X_0 \approx \frac{A \cdot 716.4 \text{ g/cm}^2}{\rho \cdot Z(Z+1) \ln(287/\sqrt{Z})}, \tag{1.2}$$

where A is the mass number, Z the atomic number and ρ the density.

2 Methods

It is possible to measure the scatter angles by determining the incoming and outgoing tracks of the muons using several resistive plate chambers (RPCs). By analysing the reconstructed tracks, information can be extracted regarding the differences in Z of the materials and their position and shape.

2.1 Geant4 Simulations

All the simulations were performed using Geant4, which is a toolkit for the simulation of the passage of particles through matter [13]. The muon spectrum of energies and angles was taken from CRY, a database of cosmic ray data [14], which creates a source plane for the muons, with realistic momentum distributions at sea level. It simulates 420000 muons per hour, of which about 5800 were recorded; the amount of data will be shown in terms of time of muon exposure. Each event is a single muon, and multiple muons in the same time window are not considered because in reality they would be vetoed.

The simulation geometry is represented in Figure 1. The RPCs have a sensitive area of 1×1 m^2 and 6 mm thickness. Each XY pair has a 19 mm spacing and there are 58 mm between each of the pairs. The distance between the top and the bottom layers is 548 mm. The waste drum placed in the centre is 40 cm long, has a 13 cm radius and is encased in steel with a thickness of 1.5 cm around the cylinder and 3.5 cm in its caps. The RPCs strips have a 1.5 mm pitch, and a 450 μm

intrinsic resolution, taken from the value of real RPCs, measured and published in [15]. As in that system, the simulation has six pairs of RPCs: three pairs above and three pairs below the waste drum. Figure 2 shows the muon scattering principle and setup.

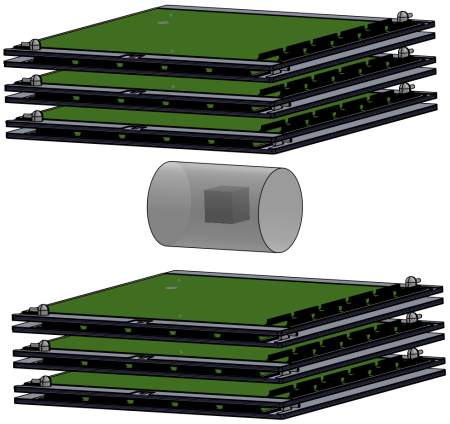

Figure 1: Illustration of the simulation geometry.

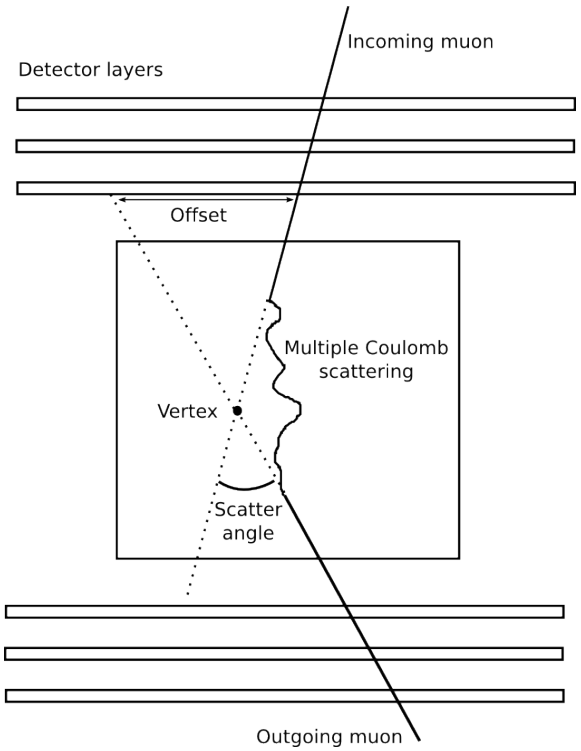

Figure 2: Illustration of the muon scattering principle and some variables obtained.

2.2 Multivariate Analysis

The output of the Geant4 simulation was then analysed by a ROOT [16] application: a fit of the upper and lower tracks (3 RPCs each, for x and y directions) was calculated using MINUIT [17]. This fit is described in [7]. The variables from this fit were analysed in order to choose the ones most sensitive to different materials. This was done by comparing the variables distributions from simple simulations of different materials irradiated by mono-energetic vertical muons. The chosen variables were then used as inputs into a multivariate analysis (MVA) to compare pairs of materials, using the ROOT package TMVA [18], more specifically using the method of Fisher's linear discriminant [19].

The variables used were the 2D projected and 3D scatter angles, the offsets – between the upper (lower) track extrapolated to the first lower (last upper) layer and the measured hit position in that layer –, the χ^2 of a six points linear track fit, the χ^2 of the combined fit of incoming and outgoing tracks, including the reconstructed vertex, and the momentum of the muon. Some of these variables are shown in Figure 3.

The MVA compared two materials each time and consisted of three steps: training, testing and application. The training was done for each block size using the same geometry as the application, taking a few seconds for each geometry. The material with highest Z was assigned as signal and the other as background.

Only the tracks that passed through the block were selected for the training from a boolean variable in the Monte Carlo which was true for each track that crossed the block. For this reason, the amount of tracks actually used was less than the recorded tracks: 10h of muon exposure for $10\times10\times10$ cm^3 and $5\times5\times5$ cm^3 blocks yielded about 26000 and 6000 selected muons respectively, 50h for the $3 \times 3 \times 3$ cm^3 and $2 \times 2 \times 2$ cm^3 blocks yielded about 12000 and 1800 muons, and 100h for the $1 \times 1 \times 1$ cm^3 block yielded about 2700 muons. Although different values were used for different geometries, it was observed that increasing the amount of data for the training would not improve the results, when using at least 1200 muons. The testing was done by TMVA with the same amount of data as the testing. For the application of MVA, the selected tracks were the ones whose reconstructed vertex was inside the block.

The 2D angles and offsets are highly correlated with the 3D angle, with linear correlation coefficients over 80%. The different χ^2 have coefficients between 50% and 70% with the 3D angle. The momentum correlates to the 3D angle by about 22% (in absolute value).

As an example, the output of the training for the Fisher discriminant comparing Uranium and Lead can be seen in Figure 4. The trained classifier was then applied to several sets of events (an event is a simulation with one cosmic muon), each set with a fixed time of muon exposure. For each set, a Fisher distribution output histogram was produced, from which discriminator values were calculated: values that should be different for signal and background, such as the mean, the integral over a cut (where the signal started being higher than the background), the integral weighted more for higher values, and the weighted integrals over and under a cut.

To evaluate the performance, ROC graphs (Receiver Operating Characteristics), which plot the true positive rate (identifying the "signal" material correctly) against the false positive rate (identifying the background material as the signal material) were produced. A detailed description of this type of graphs can be found in [20]. A measure of the quality of the discrimination performance is

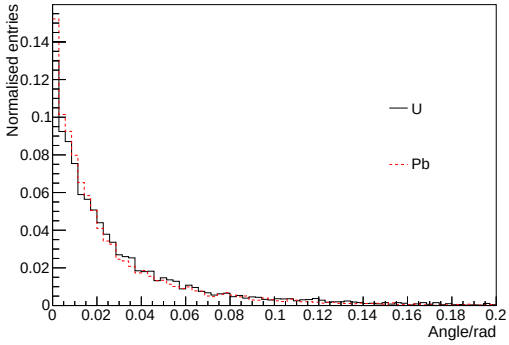

(a) Projected angle in X.

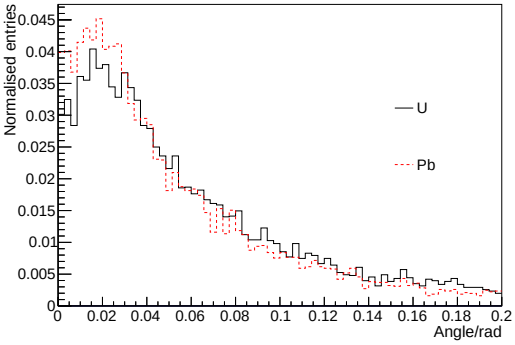

(b) 3D angle.

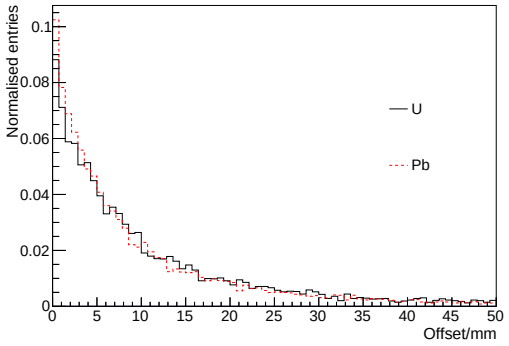

(c) Upper offset in X.

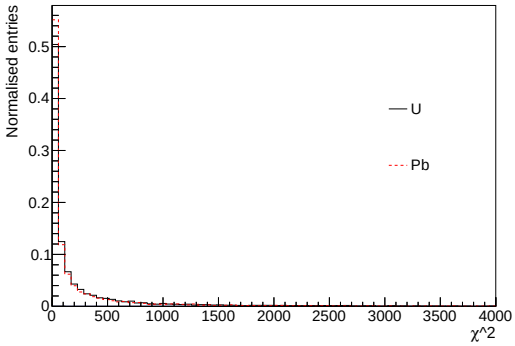

(d) Six points fit χ^2 (in X).

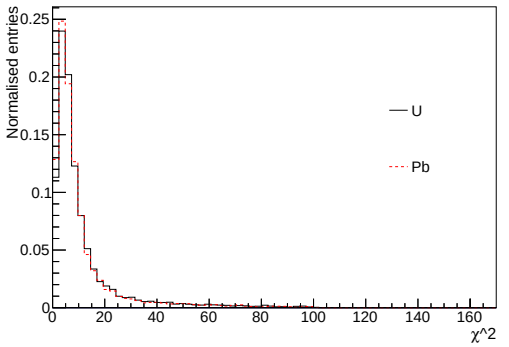

(e) Combined fit χ^2.

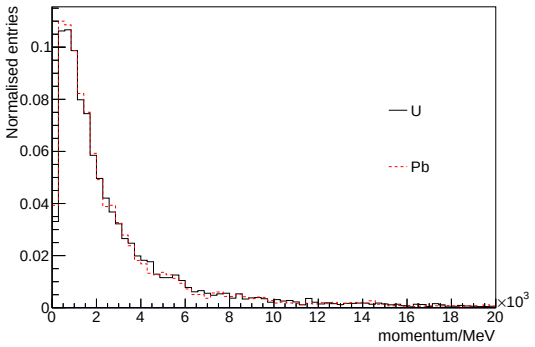

(f) Momentum.

Figure 3: Variables used in MVA training for uranium and lead, for a $10 \times 10 \times 10$ cm^3 block. The histograms are normalised to integral 1.

the area under the curve (AUC) of the ROC graphs. The AUC is shown in this paper in percentage, where 50% would correspond to a random classifier and 100% to an ideal classifier, where signal and background distributions are perfectly separated. An example of a ROC curve is in Figure 5b, distinguishing a $10 \times 10 \times 10$ cm^3 cube Uranium from Lead, for 1h of muon exposure. Each point on the curve corresponds to a cut made on each bin of the histogram in Figure 5a.

The confidence intervals of the ROC curves and respective AUC were calculated using the R package pROC [21], which uses the DeLong method described in [22].

The mean of the Fisher output showed overall higher AUC than the other discriminator values considered, therefore the mean was chosen as the discriminator for all the results. An example of the mean distributions for Uranium and Lead is in Figure 5a, where each entry of the histogram is the mean value of the Fisher discriminant method, distinguishing a $10 \times 10 \times 10$ cm^3 cube Uranium from Lead, for a set of cosmic muons of 1h exposure.. The shift to higher values of the distribution in the Uranium graph confirms that the mean is a good discriminator value.

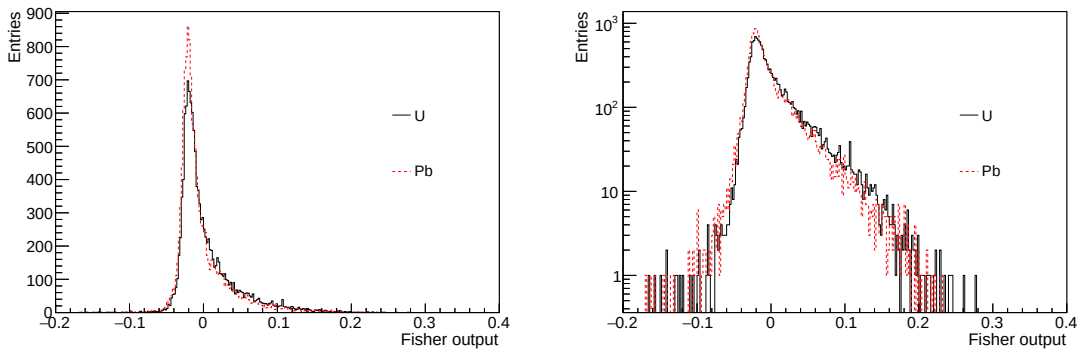

Figure 4: Output of the Fisher MVA method, comparing uranium and lead, on linear (a) and logarithmic (b) scales, to highlight the differences between the distributions, for a $10 \times 10 \times 10$ cm^3 block.

2.3 Momentum smearing

One of the variables used in the MVA is the incoming muon momentum which, combined with the angle, should show some material discrimination. This is because a large scatter angle from a high momentum muon strongly indicates localised scattering in a high-Z material, while the same large angle from a low momentum muon can also be a common scattering angle due to multiple scattering in lower-Z material.

Although it would be possible in principle using the multiple Coulomb scattering process [23], the momentum is not yet measured in our current RPC setup. Since the momentum resolution in experiments is expected to be large, the Monte-Carlo truth momentum was smeared by adding a random value from a Gaussian distribution centred in zero and with 50% of the true momentum as the standard deviation (as done in [2]). All the results used this smearing, except where stated otherwise.

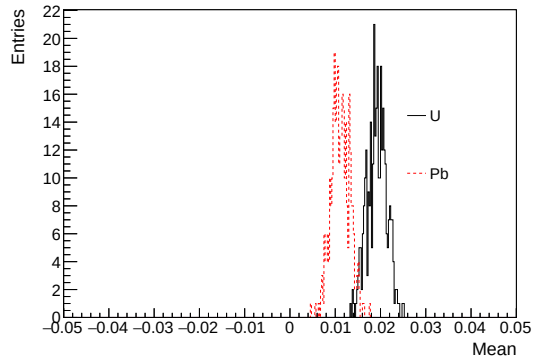

(a)

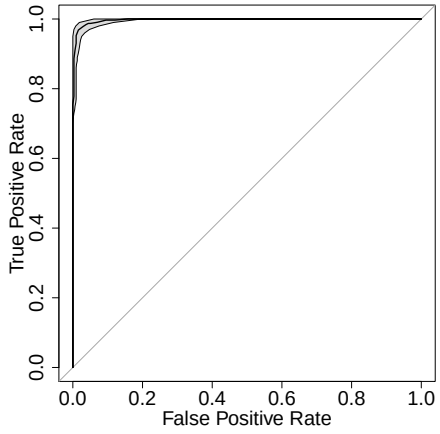

(b)

Figure 5: Mean value (a) and ROC curve (b) from the Fisher discriminant method, distinguishing Uranium from Lead, $10 \times 10 \times 10$ cm^3 cube, 1h.

A comparison was made between using the true momentum, smearing the momentum and not using the momentum information at all. As will be shown in the Results section, momentum information does not improve the method.

3 Results

Figure 6 shows the size dependence of the AUC for a fixed time (2h), where the ROC curves improve for larger blocks. Figure 7 shows the time dependence of the AUC for a block of Uranium with $5 \times 5 \times 5$ cm^3, which is almost completely distinguished from Lead after 4h.

Figure 8 shows the area under the curve of the ROC curves distinguishing Uranium from Lead (Figure 8a) and from Tungsten (Figure 8b) for different sizes and exposure times; it is clear that increasing the muon exposure time can improve the material separation.

For the smaller blocks, longer times of 10h, 40h and 70h were also tested (Figure 9). The $3 \times 3 \times 3$ cm^3 and $2 \times 2 \times 2$ cm^3 blocks show an improvement over the shorter times, so even for such small objects it is possible to have a good separation given a longer time. The the $1 \times 1 \times 1$ cm^3

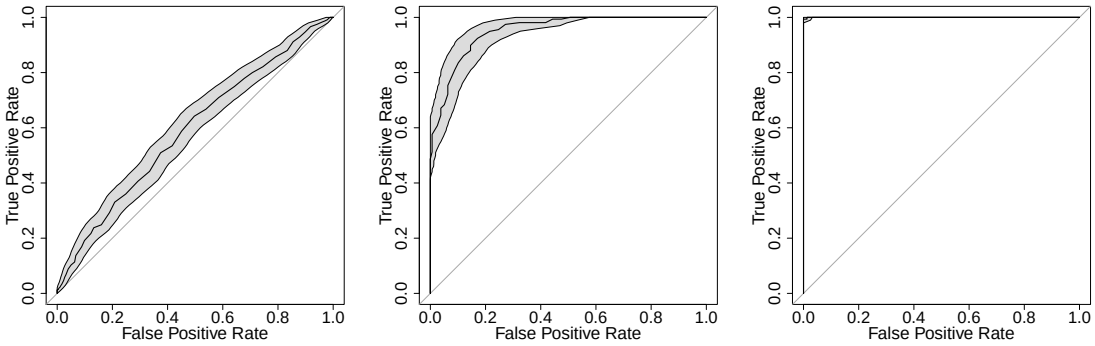

(a) $2 \times 2 \times 2$ cm^3 (b) $5 \times 5 \times 5$ cm^3 (c) $10 \times 10 \times 10$ cm^3

Figure 6: ROC curves for the mean of the Fisher determinant distinguishing Uranium from Lead for different block sizes, with a muon exposure time of 2h. The cubic blocks have a side of $2 \times 2 \times 2$ cm^3 (a), $5 \times 5 \times 5$ cm^3 (b) and $10 \times 10 \times 10$ cm^3 (c).

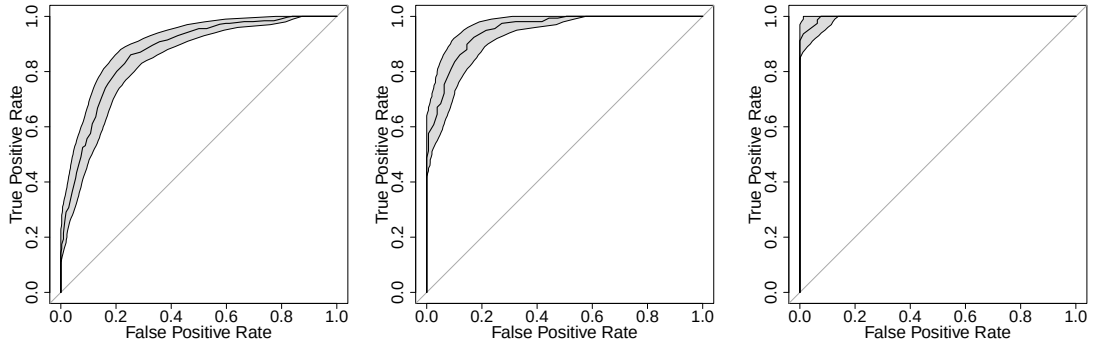

(a) 1h (b) 2h (c) 4h

Figure 7: ROC curves for the mean of the Fisher determinant distinguishing Uranium from Lead for different muon exposure times, for a cubic block with 5 cm side. The muon exposure times are 1h (a), 2h (b) and 4h (c).

does not show a significant improvement over 50%, which indicates that it would need a longer data taking time.

3.1 Results without momentum information

The momentum information, combined with the scatter angle, was expected to improve the material discrimination, by attributing more weight to a high scatter angle from a high momentum muon (more likely from a high-Z material) than from a low momentum muon. However, without momentum information, the results did not alter significantly, as can be seen by comparing the AUC of the $5 \times 5 \times 5$ cm^3 block with and without momentum information, in Table 1.

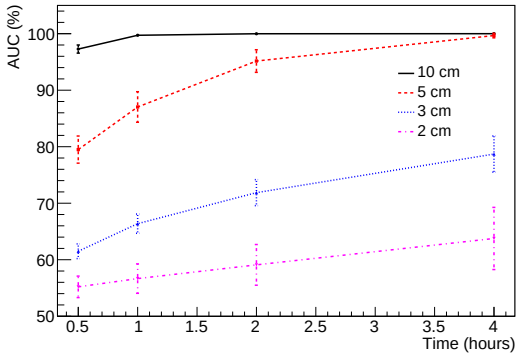

(a) Uranium vs Lead

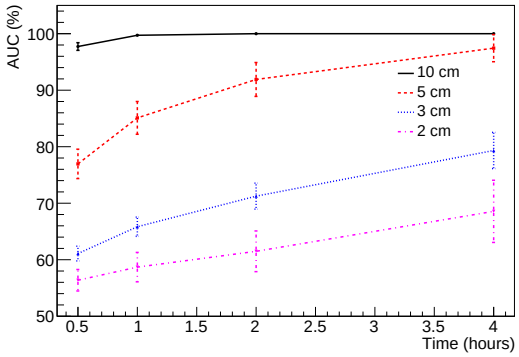

(b) Uranium vs Tungsten

Figure 8: Area under the curve of ROC curves distinguishing Uranium from Lead (a) and Uranium from Tungsten (b), for different block sizes. The error bars are the confidence intervals of the AUC.

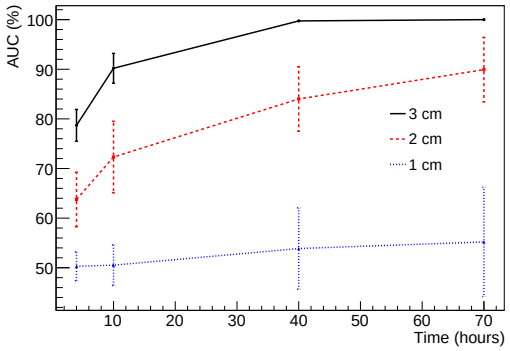

(a) Uranium vs Lead

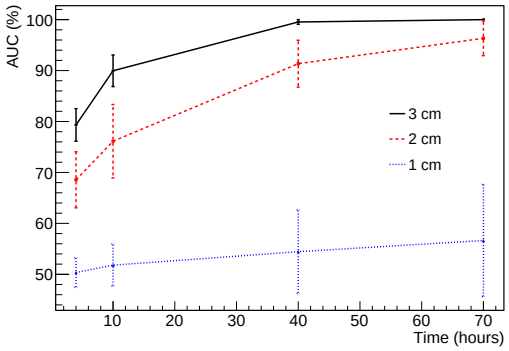

(b) Uranium vs Tungsten

Figure 9: Area under the curve of ROC curves distinguishing Uranium from Lead (a) and Uranium with Tungsten (b), for different block sizes. The error bars are the confidence intervals of the AUC.

Time	with true momentum	with momentum smearing	without momentum
1h	87.0 ± 2.7%	87.0 ± 2.7%	87.1 ± 2.7%
2h	95.2 ± 2.0%	95.2 ± 2.0%	95.3 ± 2.0%
4h	99.5 ± 0.5%	99.7 ± 0.3%	99.6 ± 0.4%

Table 1: AUC of several ROC curves from the mean of the Fisher discriminant for the $5\times5\times5$ cm^3 block, distinguishing Uranium from Lead, with and without momentum information.

3.2 Using the scatter angle instead of multiple variables

In this study, the most significant variable is the scatter angle, and almost all the others are correlated to it. Therefore, the same method used to select a material based on the mean of the Fisher output was applied to the scatter angle: for each run of a given duration, the mean of the angle was selected, and a ROC graph was plotted from all the runs of each duration. The values of AUC were compared to the ones using the Fisher discriminant. Some examples can be seen in Table 2.

Time	scatter angle	Fisher
1h	86.3 ± 2.8%	87.0 ± 2.7%
2h	94.6 ± 2.2%	95.2 ± 2.0%
4h	99.1 ± 0.9%	99.7 ± 0.3%

Table 2: AUC of several ROC curves from the mean of the scatter angle and the Fisher discriminant for the $5 \times 5 \times 5$ cm^3 block, distinguishing Uranium from Lead.

4 Discussion

This technique relies on a previous analysis, which can use longer scanning times than even the longest shown in this paper of 70h. For example, in [9] the total data taking time for a complete 3D image is 2 weeks. If the edge finding method is also used, the data taking time becomes even longer. This indicates that the method presented here does not need more data than the one already necessary for imaging.

The smallest object of $1 \times 1 \times 1$ cm^3 is under the limit of discrimination given by the angular resolution of this system.

For the training sets considered here, the use of MVA showed little or no improvement (for Lead and Tungsten respectively) over the use of the scatter angle. While MVA methods are very useful tools to combine variables, they also depend on the amount of data used for training which, combined with a set of correlated variables, can result in the same results as using only one of those variables.

5 Conclusion

Good material separation was found for blocks of at least $5 \times 5 \times 5$ cm^3 in concrete, when comparing high-Z materials to Uranium, in particular Lead and Tungsten, with 4h muon exposure using multivariate analysis to analyse muon tomography data. For smaller objects, a longer exposure time is needed: 40h is enough for the $3 \times 3 \times 3$ cm^3 block and 70h for the $2 \times 2 \times 2$ cm^3 block.

It is shown that in both cases, MVA and angle only, the knowledge of the position and shape of simple objects inside concrete can be used to discriminate between typical high-Z materials.

It is also shown that discrimination based on MVA of multiple variables provides no benefit over a simpler discrimination based on scattering angles. In addition, for the method described here, it was found that momentum information provides no benefit to material discrimination. These are important null results, which strongly inform our work moving ahead. Future work will be trying this method simulating other typical materials and verifying it with real data.

6 Acknowledgements

This work was supported by the Atomic Weapons Establishment and the Ministry of Defence. The simulations and analysis were carried out using the computational facilities of the Advanced Computing Research Centre, University of Bristol - http://www.bris.ac.uk/acrc/.

References

[1] K. N. Borozdin et al. Surveillance: Radiographic imaging with cosmic-ray muons. *Nature*, 422(March):277, 2003.

[2] C. L. Morris et al. Tomographic Imaging with Cosmic Ray Muons. *Science & Global Security*, 16(1-2):37–53, 2008.

[3] G. Jonkmans, V. N. P. Anghel, C. Jewett, and M. Thompson. Nuclear waste imaging and spent fuel verification by muon tomography. *Annals of Nuclear Energy*, 53:267–273, 2013.

[4] H. K. M. Tanaka et al. High resolution imaging in the inhomogeneous crust with cosmic-ray muon radiography: The density structure below the volcanic crater floor of Mt. Asama, Japan. *Earth and Planetary Science Letters*, 263(1-2):104–113, 2007.

[5] S. Pesente et al. First results on material identification and imaging with a large-volume muon tomography prototype. *Nuclear Instruments and Methods in Physics Research Section A: Accelerators, Spectrometers, Detectors and Associated Equipment*, 604(3):738–746, 2009.

[6] L. J. Schultz et al. Statistical reconstruction for cosmic ray muon tomography. *IEEE Transactions on Image Processing*, 16(8):1985–1993, 2007.

[7] C. Thomay et al. A binned clustering algorithm to detect high-Z material using cosmic muons. *Journal of Instrumentation*, 8(10):P10013, 2013.

[8] A. Clarkson et al. Characterising encapsulated nuclear waste using cosmic-ray muon tomography. *Journal of Instrumentation*, 10(03):P03020, 2015.

[9] C. Thomay et al. Passive 3D imaging of nuclear waste containers with Muon Scattering Tomography. *Journal of Instrumentation*, 11(03):P03008, 2016.

[10] V. L. Highland. Some practical remarks on multiple scattering. *Nuclear Instruments and Methods*, 129(2):497–499, 1975.

[11] G. R. Lynch and O. I. Dahl. Approximations to multiple Coulomb scattering. *Nuclear Instruments and Methods in Physics Research Section B: Beam Interactions with Materials and Atoms*, 58(1):6–10, 1991.

[12] K. A. Olive and Others. Review of Particle Physics. *Chin. Phys. C*, 38(9), 2014.

[13] S. Agostinelli et al. GEANT4—a simulation toolkit. *Nuclear instruments and methods in physics research section A: Accelerators, Spectrometers, Detectors and Associated Equipment*, 506(3):250–303, 2003.

[14] C. Hagmann, D. Lange, and D. Wright. Cosmic-ray shower generator (CRY) for Monte Carlo transport codes. In *Nuclear Science Symposium Conference Record, 2007. NSS'07. IEEE*, volume 2, pages 1143–1146. IEEE, 2007.

[15] P. Baesso et al. A high resolution resistive plate chamber tracking system developed for cosmic ray muon tomography. *Journal of Instrumentation*, 8(08):P08006, 2013.

[16] R. Brun and F. Rademakers. ROOT—an object oriented data analysis framework. *Nuclear Instruments and Methods in Physics Research Section A: Accelerators, Spectrometers, Detectors and Associated Equipment*, 389(1):81–86, 1997.

[17] F James and M. Roos. MINUIT - A system for function minimization and analysis of the parameter errors and correlations. *Computer Physics Communications*, 10(6):343–367, 1975.

[18] P. Speckmayer, A. Höcker, J. Stelzer, and H. Voss. The toolkit for multivariate data analysis, TMVA 4. In *Journal of Physics: Conference Series*, volume 219, page 032057. IOP Publishing, 2010.

[19] R. A. Fisher. The use of multiple measurements in taxonomic problems. *Annals of eugenics*, 7(2):179–188, 1936.

[20] T. Fawcett. An introduction to ROC analysis. *Pattern Recognition Letters*, 27(8):861–874, 2006.

[21] X. Robin et al. pROC: an open-source package for R and S+ to analyze and compare ROC curves. *BMC bioinformatics*, 12(1):77, 2011.

[22] E. R. DeLong, D. M. DeLong, and D. L. Clarke-Pearson. Comparing the areas under two or more correlated receiver operating characteristic curves: a nonparametric approach. *Biometrics*, 44(3):837–845, 1988.

[23] The OPERA Collaboration. Momentum measurement by the Multiple Coulomb Scattering method in the OPERA lead emulsion target. *New Journal of Physics*, 013026:13, 2011.